Transport properties of dilute α-Fe(X) solid solutions (X = C, N, O)

Thomas Schuler[1,2,*] and Maylise Nastar[2]

[1]*Department of Materials Science and Engineering, University of Illinois, Urbana-Champaign, Illinois 61801, USA*

[2]*DEN-Service de Recherches de Métallurgie Physique, CEA, Université Paris-Saclay, F-91191, Gif-sur-Yvette, France*

(Received 3 April 2016; published 3 June 2016)

We extend the self-consistent mean field (SCMF) method to the calculation of the Onsager matrix of Fe-based interstitial solid solutions. Both interstitial jumps and substitutional atom-vacancy exchanges are accounted for. A general procedure is introduced to split the Onsager matrix of a dilute solid solution into intrinsic cluster Onsager matrices, and extract from them flux-coupling ratios, mobilities, and association-dissociation rates for each cluster. The formalism is applied to vacancy-interstitial solute pairs in α-Fe (VX pairs, X = C, N, O), with *ab initio* based thermodynamic and kinetic parameters. Convergence of the cluster mobility contribution gives a controlled estimation of the cluster definition distance, taking into account both its thermodynamic and kinetic properties. Then, the flux-coupling behavior of each VX pair is discussed, and qualitative understanding is achieved from the comparison between various contributions to the Onsager matrix. Also, the effect of low-activation energy second-nearest-neighbor interstitial solute jumps around a vacancy on these results is addressed.

DOI: 10.1103/PhysRevB.93.224101

I. INTRODUCTION

α-Fe always contains interstitial impurities, for instance C, N, and O, either as impurities or as alloying elements. It is known that these solutes strongly bind with vacancies (V) in the body-centered-cubic (bcc) Fe matrix [1–5], where these solutes are preferentially located on interstitial octahedral sites [5]. The V-X interaction (X = C, N, or O) is so strong that at equilibrium, minor quantities of these solutes increase the total equilibrium V concentration in the solid solution by several orders of magnitude [6]. Because of this strong interaction, it is suspected that interstitial solutes affect kinetic properties of vacancies, and vice versa.

Kinetic properties of vacancies are key to understanding out-of-equilibrium phenomena in which V supersaturation (and hence V fluxes to point defect sinks) is created: quenching, irradiation. In such systems, two aspects of the kinetics must be understood: first one is to know if solutes increase or decrease V fluxes and, second one is to know whether or not the V flux induces solute redistribution. The latter phenomenon is denoted as flux coupling. It was first predicted by Anthony [7] from the analysis of quenched materials [8–10] and then observed in irradiated materials [11–13]. It is of high importance for nuclear industry as solute redistribution leads to radiation-induced segregation [14] and radiation-induced precipitation [15,16] that can alter the mechanical properties of the material [17,18]. In thermochemical diffusion processes like carburizing and nitriding of steels, interstitial solutes are diffused into metal surfaces. The flux of these elements from the surface into the bulk may induce a vacancy flux that could produce nonequilibrium V redistribution and possibly the formation of voids. Thus, the modeling of these flux-coupling phenomena is of interest for both manufacturing processes and steel applications in out-of-equilibrium conditions.

Flux coupling is generally studied in the thermodynamics of irreversible processes framework (see [14] for a review). For binary systems AB, this formalism can be summarized in the following equation:

$$\begin{pmatrix} \bar{J}^A \\ \bar{J}^B \end{pmatrix} = -\begin{pmatrix} L_{AA} & L_{AB} \\ L_{BA} & L_{BB} \end{pmatrix} \begin{pmatrix} \frac{\nabla\mu^A}{k_B T} \\ \frac{\nabla\mu^B}{k_B T} \end{pmatrix}, \tag{1}$$

where $\bar{J}^\alpha$ is the macroscopic flux of species α ($\alpha = A, B$) resulting from some driving forces, in this case expressed as chemical potential gradients $\nabla\mu^\alpha/k_B T$. The coefficients in-between fluxes and driving forces form the Onsager matrix and contain all the kinetic information related to this system. Equation (1) says that in the simplified scenario where there is only one driving force ($\nabla\mu^A \neq 0$ and $\nabla\mu^B = 0$), two fluxes are expected, $\bar{J}^A = -L_{AA}\nabla\mu^A/k_B T$ and $\bar{J}^B = -L_{BA}\nabla\mu^A/k_B T = \bar{J}^A L_{BA}/L_{AA}$. Physically, the flux of B is induced by the flux of A. This corresponds to the so-called flux-coupling phenomenon, and L_{BA}/L_{AA} is denoted as a flux-coupling coefficient, which is either positive or negative.

From a modeling point of view, flux coupling has been actively studied and is now well understood for substitutional solutes diffusing via vacancy-mediated [19–21] or dumbbell mechanisms [22–25]. For instance, in vacancy-mediated diffusion, the fact that substitutional solutes must exchange with V to move is at the origin of flux coupling between V and substitutional solutes. When it comes to interstitial solutes, which diffuse via interstitial migration on a sublattice (interstitial sites) different from that of vacancies (substitutional sites), it is not obvious to give a ruling about whether or not this system will produce some flux coupling. VX flux-coupling experiments in α-Fe are difficult to perform because solute solubility limits are very low, and measuring the flux-coupling contribution to segregation is a challenging task. Hence, we must turn to modeling to answer these questions.

The thermodynamics of α-Fe-V-X systems is now well understood and can be studied further using well-defined numerical and analytical modeling methods [5,6]. Assessing the kinetic properties of such system is a much more difficult problem. Early studies of the kinetic interplay between defects and interstitial solutes were related to the trapping of hydrogen atoms in Fe [26,27]. These models assume the solute to be immobile in the trap sites until it manages to escape, and the

*Corresponding author; tschul@illinois.edu

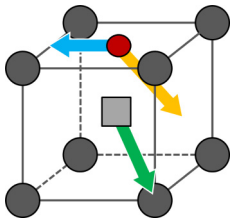

FIG. 1. Drawing of the three types of jumps considered in this paper: vacancy (gray square) and Fe matrix atom exchange (green arrow parallel to the $[1\bar{1}\bar{1}]$ direction), jump between two NN interstitial octahedral sites (blue arrow parallel to the $[\bar{1}00]$ direction), and jump between two second-NN interstitial octahedral sites around a vacancy (orange arrow parallel to the $[1\bar{1}0]$ direction).

effect of this trapping phenomenon on the overall diffusivity of the solute is a function of the solute-trap interaction enthalpy only. More recent contributions have included the possibility that solute could move within traps (see, e.g., [28,29]), but one still needs to compute the kinetic properties of trapped solutes. A model to do that has been proposed by Koiwa, using a first-passage time approach [30], but this model is limited to first-nearest-neighbor (NN) trap-solute interaction (both for stable and saddle-point configurations). Trapping effects have also been addressed the other way around, in the case where vacancies are trapped by interstitial solutes, thus affecting the iron self-diffusion coefficient [31–33]. Some authors claim that interstitial solutes increase the Fe diffusion coefficient [34], while others claim the opposite [35], but it is not always made clear whether or not the effect of solutes on vacancy equilibrium concentration is accounted for in these studies.

Nowadays, there are *ab initio* data that give an accurate picture of the local energetic landscape in various configurations [36]. For substitutional solutes, there are simple models [37,38] and more complicated ones [20,21] that can transform this *ab initio* data into statistically averaged and macroscopically well-defined kinetic coefficients. With interstitial solute, one has to deal with two simultaneous migration mechanisms happening on two different sublattices (see Fig. 1) but affecting each other through local energetic landscape modifications. Because of that, the problem becomes much more complicated, and has not been addressed yet. Moreover, it has been shown that interstitial solutes can perform low-activation second-NN jumps in the vicinity of V (see Fig. 1), which is an additional complication for modeling [36]. To the best of the authors' knowledge, there is currently no model to take into account the full kinetic interplay between vacancies and interstitial solutes because these can eventually move altogether in a complicated energetic landscape, and the consequence on the kinetic properties of the system cannot be reduced to a simple thermodynamic trapping enthalpy. Moreover, such model would give mobility coefficients of defect-solute clusters, a valuable information for higher-scale models such as object kinetic Monte Carlo [39] or cluster dynamics [3,36].

The self-consistent mean field method (SCMF) is a promising path to provide kinetic models for α-Fe-V-X systems. First developed for vacancy-mediated diffusion in bcc lattices, it has since then been extended to various cases [20,21,40–47], but these always considered substitutional migration mechanisms only. Basically, the SCMF method uses linear response theory to compute the flux resulting from a uniform driving force, which allows the identification of the Onsager matrix. It is based on a microscopic master equation, and thus provides a general way to link atomic-scale information (atomic jump frequencies) to macroscopic transport coefficients. The same formalism has also been extended to include the effect of nonuniform driving forces [47].

In this paper, we make use of the SCMF method to provide an exact kinetic model for α-Fe-V-X dilute systems, and use this model to study flux couplings in this system. Section II is devoted to theoretical developments. We derive the SCMF equations for various jump mechanisms on various sublattices, and then propose a breakdown of the Onsager matrix of dilute alloys into cluster contributions. Section III uses these theoretical developments. First, we present the parametrization of our model, and then we discuss the convergence of the mobility contribution with respect to cluster size. From this, we were able to investigate intrinsic flux-coupling coefficients of VX pairs, and quantify the effect of second-NN solute jumps around V. Finally, Sec. IV provides an insightful comparison between various approximations of cluster kinetic coefficients.

II. EXTENSION OF THE SCMF METHOD

A. SCMF for various jump mechanisms on various sublattices

In this section, we propose an extension of the self-consistent mean field method (SCMF), first developed in [44] for solute migration by vacancy mechanism in bcc solids, to systems containing different diffusion mechanisms on various sublattices. In Sec. III, we will apply this method to the case of vacancy and interstitial solute (C, N, and O) migration in α-Fe. To the best of the authors' knowledge, there exists no analytical model to compute transport coefficients in such systems. Moreover, the extension proposed in this paper is readily applicable to many other complex diffusive systems. It piles up with a number of papers that have developed various extensions of the SCMF method over the past decade [20,21,40–47], and it provides the first theoretical steps toward a rigorous definition of kinetic variables associated with point-defect-solute clusters, making it a method of growing interest, generality, and efficiency. We chose to derive the SCMF equations from scratch to have a self-consistent paper. Moreover, it will be easier to introduce our notations, as well as the features of our extension. The general idea of the method is to apply a small driving force to the system, a chemical potential gradient, and to compute the resulting flux in a linear approximation. The coefficients that relate fluxes to driving forces at steady state are then identified as the transport coefficients in the framework of the thermodynamics of irreversible processes [see Eq. (1)].

It is assumed that the system can be mapped onto a rigid lattice containing a number of lattice sites, each being occupied by a single atom or defect. The derivation starts from the microscopic master equation for a system represented by a configuration vector $\mathbf{n}$ which components are the site occupation numbers n_i^α for each site and each species. $n_i^\alpha = 1$ if species α occupies site i in configuration $\mathbf{n}$, and $n_i^\alpha = 0$ if not:

$$\frac{dP(\mathbf{n},t)}{dt} = \sum_{\tilde{\mathbf{n}}} [W(\tilde{\mathbf{n}},\mathbf{n})P(\tilde{\mathbf{n}},t) - W(\mathbf{n},\tilde{\mathbf{n}})P(\mathbf{n},t)]. \quad (2)$$

$P(\mathbf{n},t)$ is the probability of having configuration $\mathbf{n}$ at time t, and $W(\tilde{\mathbf{n}},\mathbf{n})$ is the rate $[s^{-1}]$ at which a system in configuration $\tilde{\mathbf{n}}$ switches to configuration $\mathbf{n}$. As in Ref. [45], it is assumed that the probability of any configuration can be expressed as the product of its equilibrium probability $P_0(\mathbf{n})$ and a probability $\delta P(\mathbf{n},t)$ that corresponds to the deviation from equilibrium,

$$P(\mathbf{n},t) = P_0(\mathbf{n}) \times \delta P(\mathbf{n},t). \tag{3}$$

The $\delta P(\mathbf{n},t)$ probability is assumed to have the same mathematical form as the equilibrium probability, but thermodynamic interactions are replaced by an effective Hamiltonian that will reproduce the fact that two equivalent configurations at equilibrium do not necessarily have the same probability in out-of-equilibrium conditions (and this is because driving forces break the symmetry of the system). In this paper, the effective Hamiltonian is reduced to pair effective interactions $v_{ij}^{\alpha\beta}$ between sites i and j, occupied, respectively, by species α and β:

$$\delta P(\mathbf{n},t) = \exp\left[\left(\delta\Omega(t) + \sum_i \sum_\alpha n_i^\alpha \delta\mu_i^\alpha(t) - \frac{1}{2}\sum_{i,j}\sum_{\alpha,\beta} n_i^\alpha n_j^\beta v_{ij}^{\alpha\beta}(t)\right)\Big/ k_B T\right]. \tag{4}$$

$\delta\mu_i^\alpha(t)$ is the local (site i) deviation from the equilibrium chemical potential of species α and $\delta\Omega(t)$ is a normalizing constant.

The continuity equation reads as

$$\frac{d[\alpha]_i}{dt} = -\nabla J_i^\alpha, \tag{5}$$

where $[\alpha]_i$ is the probability of site i to be occupied by species α (hence the local site concentration), J_i^α is the microscopic flux of species α from site i, and ∇ is the divergence operator. The concentration of species α on site i is also given by the first moment of the probability distribution:

$$[\alpha]_i = \langle n_i^\alpha \rangle = \sum_{\mathbf{n}} n_i^\alpha P(\mathbf{n},t). \tag{6}$$

$\langle \ldots \rangle$ denotes the ensemble average over the probability distribution $P(\mathbf{n},t)$. Using the discrete divergence operator, we get

$$\frac{d\langle n_i^\alpha \rangle}{dt} = -\sum_{s\epsilon\theta_i^\alpha} J_{i\to s}^\alpha, \tag{7}$$

where θ_i^α is the ensemble containing all sites where an atom of species α located on site i can jump to. Equation (7) provides an expression for the microscopic flux, so we need to evaluate the time derivative of the local concentration. Following, we write the step-by-step derivation for vacancies ($\alpha = V$):

$$\frac{d\langle n_i^V \rangle}{dt} = \frac{d}{dt}\left(\sum_{\mathbf{n}} n_i^V P(\mathbf{n},t)\right) = \sum_{\mathbf{n}} n_i^V \frac{dP(\mathbf{n},t)}{dt}. \tag{8}$$

This equation stems from the definition (6). Then, Eqs. (2), (3), and detailed balance at equilibrium [$W(\tilde{\mathbf{n}},\mathbf{n})P_0(\tilde{\mathbf{n}},t) = W(\mathbf{n},\tilde{\mathbf{n}})P_0(\mathbf{n},t)$] are inserted in Eq. (8):

$$\begin{aligned}\frac{d\langle n_i^V \rangle}{dt} &= \sum_{\mathbf{n},\tilde{\mathbf{n}}} n_i^V [W(\tilde{\mathbf{n}},\mathbf{n})P(\tilde{\mathbf{n}},t) - W(\mathbf{n},\tilde{\mathbf{n}})P(\mathbf{n},t)] \\ &= \sum_{\mathbf{n},\tilde{\mathbf{n}}} n_i^V W(\mathbf{n},\tilde{\mathbf{n}})P_0(\mathbf{n})[\delta P(\tilde{\mathbf{n}},t) - \delta P(\mathbf{n},t)] \\ &= \left\langle \sum_{\tilde{\mathbf{n}}} n_i^V W(\mathbf{n},\tilde{\mathbf{n}})[\delta P(\tilde{\mathbf{n}},t) - \delta P(\mathbf{n},t)] \right\rangle^{(0)},\end{aligned} \tag{9}$$

where $\langle \ldots \rangle^{(0)}$ denotes the ensemble average over the equilibrium probability distribution $P_0(\mathbf{n},t)$. Then, we expand Eq. (4) to first order for small deviations from equilibrium, and evaluate $\delta P(\tilde{\mathbf{n}},t) - \delta P(\mathbf{n},t)$:

$$\frac{d\langle n_i^V \rangle}{dt} = \frac{1}{k_B T}\left\langle \sum_{\tilde{\mathbf{n}}} n_i^V W(\mathbf{n},\tilde{\mathbf{n}})\left[\sum_{j,\alpha}\left(\tilde{n}_j^\alpha - n_j^\alpha\right)\delta\mu_k^\gamma - \frac{1}{2}\sum_{j,k,\alpha,\gamma}\left(\tilde{n}_j^\alpha \tilde{n}_k^\gamma - n_j^\alpha n_k^\gamma\right)v_{jk}^{\alpha\gamma}\right]\right\rangle^{(0)}. \tag{10}$$

One must be aware of the fact that all nonzero terms in the equilibrium ensemble average are those for which V is at site i in configuration $\mathbf{n}$. If we consider transitions between two configurations $\tilde{\mathbf{n}}$ and $\mathbf{n}$ where the vacancy at site i does not move, then all the terms in the bracket will cancel out when $\tilde{\mathbf{n}}$ and $\mathbf{n}$ are inverted in the double sum over all configurations of the system (one sum is written explicitly, while the other is implicit in the $\langle \ldots \rangle^{(0)}$ symbol). Thus, the sum over $\tilde{\mathbf{n}}$ is restricted to configurations where V is one jump away from site i, and jumps of the vacancy towards these neighboring sites are the only transitions that do not cancel out. A denotes matrix atoms:

$$\begin{aligned}&\frac{d\langle n_i^V \rangle}{dt} \\ &= \frac{1}{k_B T}\left\langle n_i^V \sum_{s\epsilon\theta_i^V} n_s^A \omega_{is}^{VA}\left[\left(\delta\mu_i^A + \delta\mu_s^V - \delta\mu_i^V - \delta\mu_s^A\right) + 2v_{is}^{VA} - \sum_{k\neq i\neq s,\gamma} n_k^\gamma\left(v_{ik}^{A\gamma} + v_{sk}^{V\gamma} - v_{ik}^{V\gamma} - v_{sk}^{A\gamma}\right)\right]\right\rangle^{(0)}.\end{aligned} \tag{11}$$

As only differences in chemical potentials appear, the following notation is used: $\delta\bar{\mu}_i^V = \delta\mu_i^V - \delta\mu_i^A$. For the sake of simplicity, we assume that effective interactions with matrix atoms are null because they only shift the reference value for effective interactions and do not affect the final result. Thus, the only nonzero effective interactions are between V and X. Lastly, it is assumed that the driving force is homogeneous in the system and we define $d_{is}\nabla\bar{\mu}^V = \vec{\lambda}_{is}.\vec{\nabla}\bar{\mu}^V$, where $\vec{\lambda}_{is}$ is the jump vector between sites i and s. It follows that effective interactions v_{ik}^{VX} can be grouped into classes of effective interactions $\sigma(ik)$ that obey translational invariance, and are

fully determined by the $\vec{ik}$ vector:

$$\frac{d\langle n_i^V\rangle}{dt} = \sum_{s\epsilon\theta_i^V}\left\langle n_i^V n_s^A \omega_{is}^{VA}\left[\frac{\delta\bar{\mu}_s^V - \delta\bar{\mu}_i^V}{k_BT} + \sum_k n_k^X \frac{\nu_{ik}^{VX} - \nu_{sk}^{VX}}{k_BT}\right]\right\rangle^{(0)} = \sum_{s\epsilon\theta_i^V}\left\langle n_i^V n_s^A \omega_{is}^{VA}\left[d_{is}\frac{\nabla\bar{\mu}^V}{k_BT} + \sum_k n_k^X \frac{\nu_{\sigma(ik)}^{VX} - \nu_{\sigma(sk)}^{VX}}{k_BT}\right]\right\rangle^{(0)}. \quad (12)$$

Finally, comparing the last line of Eq. (12) with Eq. (7), one can identify the expression for the microscopic flux between sites i and s:

$$-J_{i\to s}^V = \left\langle n_i^V n_s^A \omega_{is}^{VA}\left(d_{is}\frac{\nabla\bar{\mu}^V}{k_BT} + \sum_k n_k^X \frac{\nu_{\sigma(ik)}^{VX} - \nu_{\sigma(sk)}^{VX}}{k_BT}\right)\right\rangle^{(0)}. \quad (13)$$

The exact same derivation can be done for the migration of interstitial solutes on the sublattice containing interstitial octahedral sites. The same arguments apply, but interstitial solutes X exchange with interstitial vacancies ζ. In Eq. (13), substituting V into X and A into ζ leads to

$$-J_{i\to s}^X = \left\langle n_i^X n_s^\zeta \omega_{is}^{X\zeta}\left(d_{is}\frac{\nabla\bar{\mu}^X}{k_BT} + \sum_k n_k^V \frac{\nu_{\sigma(ik)}^{XV} - \nu_{\sigma(sk)}^{XV}}{k_BT}\right)\right\rangle^{(0)}. \quad (14)$$

Please note that Eqs. (13) and (14) only represent microscopic fluxes between two lattice sites. Macroscopic fluxes, i.e., those entering Eq. (1), projected along the chemical potential gradient are obtained as

$$\overline{J}^\alpha = \frac{1}{S_\perp^\alpha}\sum_{s\epsilon\theta_{i+}^\alpha} J_{i\to s}^\alpha, \quad (15)$$

where $S_\perp^\alpha$ is the unit surface per atom α perpendicular to the chemical potential gradient, and θ_{i+}^α is a subset of θ_i^α, restricted to sites s for which $\vec{\lambda}_{is}.\vec{\nabla}\bar{\mu}^\alpha > 0$.

The unknowns in Eqs. (13) and (14) are the effective interactions, and this is why this method is called self-consistent. Indeed, the effective interactions are obtained from the steady-state condition of the second moment of the out-of-equilibrium probability distribution

$$\frac{d\langle n_i^V n_j^X\rangle}{dt} = \sum_{s\epsilon\theta_i^V}\left\langle n_j^X n_i^V n_s^A \omega_{is}^{VA}\left[d_{is}\frac{\nabla\bar{\mu}^V}{k_BT} + \frac{\nu_{\sigma(ij)}^{VX} - \nu_{\sigma(sj)}^{VX}}{k_BT}\right]\right\rangle^{(0)} + \sum_{s\epsilon\theta_j^X}\left\langle n_i^V n_j^X n_s^\zeta \omega_{js}^{X\zeta}\left[d_{js}\frac{\nabla\bar{\mu}^X}{k_BT} + \frac{\nu_{\sigma(ji)}^{XV} - \nu_{\sigma(si)}^{XV}}{k_BT}\right]\right\rangle^{(0)} = 0, \quad (16)$$

which is rewritten in a more convenient form

$$\sum_{s\epsilon\theta_i^V}\left\langle n_j^X n_i^V n_s^A \omega_{is}^{VA} d_{is}\right\rangle^{(0)}\nabla\bar{\mu}^V + \sum_{s\epsilon\theta_j^X}\left\langle n_i^V n_j^X n_s^\zeta \omega_{js}^{X\zeta} d_{js}\right\rangle^{(0)}\nabla\bar{\mu}^X = \sum_{s\epsilon\theta_i^V}\left\langle n_j^X n_i^V n_s^A \omega_{is}^{VA}\left(\nu_{\sigma(sj)}^{VX} - \nu_{\sigma(ij)}^{VX}\right)\right\rangle^{(0)} + \sum_{s\epsilon\theta_j^X}\left\langle n_i^V n_j^X n_s^\zeta \omega_{js}^{X\zeta}\left(\nu_{\sigma(is)}^{VX} - \nu_{\sigma(ij)}^{VX}\right)\right\rangle^{(0)}. \quad (17)$$

If all the terms corresponding to a given effective interaction class are grouped together, a more compact form can be obtained:

$$\sum_\alpha m_{ij,\alpha}^{VX}\nabla\bar{\mu}^\alpha = \sum_\sigma t_{ij,\sigma}^{VX}\nu_\sigma^{VX}. \quad (18)$$

Equation (16) must be computed for each pair of sites i and j corresponding to an effective interaction class $\sigma(ij)$, which will give as many different equations as the number of effective interaction classes. Thus, all of these can be rewritten in a matrix form, showing that the effective interaction classes contained in vector $\boldsymbol{K}$ are the solutions to a linear system, and require the inversion of matrix $\boldsymbol{T}$:

$$\boldsymbol{T}\cdot\boldsymbol{K} = \boldsymbol{M}\cdot\begin{pmatrix}\nabla\bar{\mu}^V\\ \nabla\bar{\mu}^X\end{pmatrix}. \quad (19)$$

Moreover, this linear system shows that the effective interaction classes are linear with respect to the chemical potential gradients of each species. Then, Eq. (15) can also be written in a matrix form

$$\overline{J}^\alpha = -\frac{1}{S_\perp^\alpha}\sum_{s\epsilon\theta_{i+}^\alpha}\left[\boldsymbol{\Lambda}_0^\alpha\cdot\begin{pmatrix}\frac{\nabla\bar{\mu}^V}{k_BT}\\ \frac{\nabla\bar{\mu}^X}{k_BT}\end{pmatrix} + \frac{1}{k_BT}\boldsymbol{\Lambda}^\alpha\cdot\boldsymbol{K}\right] = -\frac{1}{S_\perp^\alpha}\sum_{s\epsilon\theta_{i+}^\alpha}\left[\boldsymbol{\Lambda}_0^\alpha + \boldsymbol{\Lambda}^\alpha\cdot\boldsymbol{T}^{-1}\cdot\boldsymbol{M}\right]\begin{pmatrix}\frac{\nabla\bar{\mu}^V}{k_BT}\\ \frac{\nabla\bar{\mu}^X}{k_BT}\end{pmatrix}. \quad (20)$$

All terms in matrices $\boldsymbol{\Lambda}_0^\alpha$, $\boldsymbol{\Lambda}^\alpha$, $\boldsymbol{T}$, and $\boldsymbol{M}$ are linear combinations of jump frequencies $\omega_{is}^{\alpha\beta}$, such that the final expression of the macroscopic flux $\overline{J}^\alpha$ is a linear combination of driving forces, from which it is possible to identify transport coefficients $L_{\alpha V}$ and $L_{\alpha X}$.

In the initial formulation of the SCMF method [44,45], effective interactions are shown to be antisymmetric in a homogeneous chemical potential gradient: $\nu_{ij}^{\alpha\beta} = -\nu_{ij}^{\beta\alpha} = -\nu_{ji}^{\alpha\beta} = \nu_{ji}^{\beta\alpha}$. Because of this, effective interactions were differentiated by bond length and bond projection along the chemical potential gradient direction in previous studies using the SCMF (e.g., [20,21]). One must be aware that in some systems, i.e., the α-Fe-V-X system, other criteria used to differentiate between kinetic interaction classes must be added. In this work, effective interactions that are part of a given class share the same symmetry with respect to the crystal and the chemical potential gradient direction, which includes previous criteria.

Analytical expressions for matrices $\mathbf{\Lambda}_0^\alpha$, $\mathbf{\Lambda}^\alpha$, $\boldsymbol{T}$, and $\boldsymbol{M}$ are provided in Appendix A.

B. Breakdown of transport coefficients into cluster contributions

The major advantage of the SCMF theory is that it gives analytical expressions for transport coefficients as a function of atomic jump rates. These expressions enable to reach a much deeper understanding of the kinetics of the system than macroscopic transport coefficients provide. In order to keep the discussion simple, we restrict ourselves to the purpose of this paper: investigating the kinetic properties of an infinitely dilute system, i.e., a α-Fe matrix in which vacancy-solute clusters larger than VX pairs are neglected, and V clusters and X clusters are neglected. Let us define a distance called the pair definition radius and denoted R. For now, this definition is arbitrary, but below we set up a framework to define this distance more rigorously.

For a given configuration $\mathbf{n}$, every jump rate $\omega_{is}^{\alpha\beta}$ that appears in the SCMF equations can be assigned to a given cluster:

(i) If V (resp. X) is isolated before and after the jump (meaning that there are no X nor V at a distance lower than R from sites i and s), the corresponding jump frequency is related to the migration of an isolated V (resp. X).

(ii) If before and/or after the jump there is a solute (resp. V) near (meaning at a distance lower than R from sites i or s) the jumping V (resp. X), the corresponding jump frequency is related to the VX pair cluster.

Thus, in our dilute system, there are three cluster contributions to the total Onsager matrix:

$$\begin{pmatrix} L_{VV} & L_{VX} \\ L_{XV} & L_{XX} \end{pmatrix} = \begin{pmatrix} \tilde{L}_{VV}(V) & 0 \\ 0 & 0 \end{pmatrix} + \begin{pmatrix} 0 & 0 \\ 0 & \tilde{L}_{XX}(X) \end{pmatrix} + \begin{pmatrix} \tilde{L}_{VV}(VX) & \tilde{L}_{VX}(VX) \\ \tilde{L}_{XV}(VX) & \tilde{L}_{XX}(VX) \end{pmatrix}. \quad (21)$$

At equilibrium, for each cluster c_i (concentration per unit volume $[c_i]^{eq}$), we define cluster transport coefficients $L_{\alpha\beta}(c_i)$:

$$L_{\alpha\beta}(c_i) = \frac{\tilde{L}_{\alpha\beta}(c_i)}{[c_i]^{eq}}. \quad (22)$$

This way, the Onsager matrix for the total system is now an explicit function of V monomers, X monomers, and VX pairs concentrations ($[V]$, $[X]$, and $[VX]$, respectively):

$$\begin{pmatrix} L_{VV} & L_{VX} \\ L_{XV} & L_{XX} \end{pmatrix} = [V]\begin{pmatrix} L_{VV}(V) & 0 \\ 0 & 0 \end{pmatrix} + [X]\begin{pmatrix} 0 & 0 \\ 0 & L_{XX}(X) \end{pmatrix} + [VX]\begin{pmatrix} L_{VV}(VX) & L_{VX}(VX) \\ L_{XV}(VX) & L_{XX}(VX) \end{pmatrix}. \quad (23)$$

At thermal equilibrium ($[c_i] = [c_i]^{eq}$), Eqs. (21) and (23) are rigorously equivalent. Let us now emphasize the fact that the SCMF method produces thermodynamic averages $\langle n_i^V n_s^A \omega_{is}^{VA} \rangle^{(0)}$ meaning that the products $P_0(\mathbf{n})W(\mathbf{n},\tilde{\mathbf{n}})$ are the relevant microscopic quantities for transport coefficients, not the atomic jump rates alone. Let $\Omega(c_i)$ be the ensemble containing all configurations $\mathbf{n}$ of the system in which V and X are at most at distance R from each other. Then, the equilibrium concentration of cluster c_i is expressed as

$$[c_i]^{eq} = \frac{1}{V_{at}} \sum_{\mathbf{n}\in\Omega(c_i)} P_0(\mathbf{n}), \quad (24)$$

where V_{at} is the atomic volume. From Eqs. (22) and (24), thermodynamic averages $\langle n_i^V n_s^A \omega_{is}^{VA} \rangle^{(0)}$ in cluster transport coefficients $L_{\alpha\beta}(c_i)$ are functions of the microscopic quantities $V_{at}\eta(\mathbf{n})W(\mathbf{n},\tilde{\mathbf{n}})$, where

$$\eta(\mathbf{n}) = \frac{P_0(\mathbf{n})}{\sum_{\mathbf{n}\in\Omega(c_i)} P_0(\mathbf{n})}. \quad (25)$$

A cluster is made of various microscopic configurations $\mathbf{n}$, and $\eta(\mathbf{n})$ gives the probability of these microscopic concentrations with respect to the probability of the whole cluster. From these developments, it stems that cluster transport coefficients $L_{\alpha\beta}(c_i)$ are intrinsic equilibrium properties of each cluster, and are expressed in m^2/s, like diffusion coefficient. Transport coefficients for the whole system $L_{\alpha\beta}$ may be out-of-equilibrium quantities if concentrations in Eq. (23) are not equilibrium concentrations.

From the same reasoning, we can go further in the breakdown of the Onsager matrix and split each cluster transport coefficient into two contributions, looking at the various transition rates that appear in the SCMF equations:

(i) If before and after the jump there is a solute (resp. V) near (meaning at a distance lower than R from sites i and s) the jumping V (resp. X), the corresponding jump frequency is related to the migration of the VX pair cluster.

(ii) If before or after (but not both) the jump there is a solute (resp. V) near (meaning at a distance lower than R from sites i and s) the jumping V (resp. X), the corresponding jump frequency is related to the dissociation or association of the VX pair cluster. An association jump being necessarily the reverse jump of a dissociation jump (and vice versa), it stems from detailed balance at equilibrium that the association and dissociation contributions to the overall cluster transport coefficient are equal, which is the reason why they are grouped together.

Practically, some of these coefficients are 0, so that the Onsager matrix for the dilute α-Fe-V-X system reduces to the following expression:

$$\begin{pmatrix} L_{VV} & L_{VX} \\ L_{XV} & L_{XX} \end{pmatrix} = [V]M(V)\begin{pmatrix} 1 & 0 \\ 0 & 0 \end{pmatrix} + [X]M(X)\begin{pmatrix} 0 & 0 \\ 0 & 1 \end{pmatrix} + [VX]M(VX)\begin{pmatrix} 1 & 1 \\ 1 & 1 \end{pmatrix} + [VX]\begin{pmatrix} AD_{VV}(VX) & AD_{VX}(VX) \\ AD_{XV}(VX) & AD_{XX}(VX) \end{pmatrix}. \quad (26)$$

$M(c_i)$ is the mobility of cluster c_i and $AD_{\alpha\beta}(c_i)$ is the association/dissociation contribution to the cluster transport coefficient $L_{\alpha\beta}(c_i)$. Thus, we can take advantage of the analytical SCMF expressions derived above to compute distinct transport coefficient contributions for this system, each having a clear physical meaning. From a technical point of view,

these contributions are obtained using the flux expressions [Eq. (20)], but in which all jump frequencies that do not correspond to this particular contribution are set to zero (see Table I in Appendix A for an example).

A generalized and justified explanation for the breakdown of the Onsager matrix for dilute systems will be given in Ref. [48], so here we restrain ourselves to a few comments concerning Eq. (26): the mobility of the VX pair appears to be a scalar quantity which is consistent with the idea that when a cluster moves, all of its components must move at the same pace. Flux coupling stems from kinetic correlations, and the relevant quantities for this phenomenon are the off-diagonal coefficients of the Onsager matrix. For the simple system under study, Eq. (26) clearly shows that the physics of flux coupling is fully contained into two contributions: the mobility of the pair (which necessarily produces positive flux coupling as both species belonging to the cluster diffuse together), and the association/dissociation term, that contains the spatial correlation between association, migration, and dissociation jumps.

In the next section, we compute the contributions appearing in Eq. (26) for each of the three solutes, and the corresponding analytical expressions are provided in Appendix A. Also, an analytical expression of $M(VX)$ is given for simplified models in Appendix B.

III. KINETIC COEFFICIENTS OF VX PAIRS IN α-FE

A. Thermodynamic and jump frequency parametrization

In order to use Eq. (20) to obtain cluster transport coefficients, one needs only to know the following:

(a) geometry of the lattice and jump vectors for each species ($\vec{\lambda}_{is}$);

(b) equilibrium probability of each microscopic configuration of the cluster ($\eta(\mathbf{n})$);

(c) jump frequencies (computed at thermal equilibrium) as a function of the local chemical environment ($\omega_{is}^{\alpha\beta}(\mathbf{n})$).

The equilibrium probability distribution can be obtained by any thermodynamic method, for instance, Bragg-Williams approximation, cluster-variation method, low-temperature expansion, or Monte Carlo sampling. Each of these methods requires some energetic model as an input. Again, the energetics of the system can be obtained in various ways: density-functional theory calculations (DFT), tight-binding potentials, semiempirical potentials, cluster expansions. Here, we refer to Ref. [5] in which DFT binding energies of VX pairs in Fe were consistently computed for $X =$ C, N, and O. Then, the equilibrium probability distribution is obtained from a low-temperature expansion of the partition function of the system, which, despite its name, works very well up to $T =$ 1185 K in this system, temperature above which the Fe matrix changes from bcc to face-centered cubic [5].

Vacancy migration energies were also computed consistently using DFT in α-Fe for V monomers, X monomers, and VX pairs [36]. From the findings of this paper, we will investigate the effect of the low-barrier second-NN jump of X around V on the overall kinetic properties of a VX pair cluster. Finally, attempt frequencies ν_0 are assumed to depend on the jumping species only, and their values are computed from diffusion prefactors measured in self-diffusion and solute tracer diffusivities experiments in α-Fe [49]: $\nu_0(V) = 6.7 \times 10^{-6}\mathrm{m}^2/\mathrm{s}, \nu_0(C) = 1.8 \times 10^{-6}\ \mathrm{m}^2/\mathrm{s}, \nu_0(N) = 5.0 \times 10^{-7}\ \mathrm{m}^2/\mathrm{s}$, and $\nu_0(O) = 1.0 \times 10^{-6}\ \mathrm{m}^2/\mathrm{s}$.

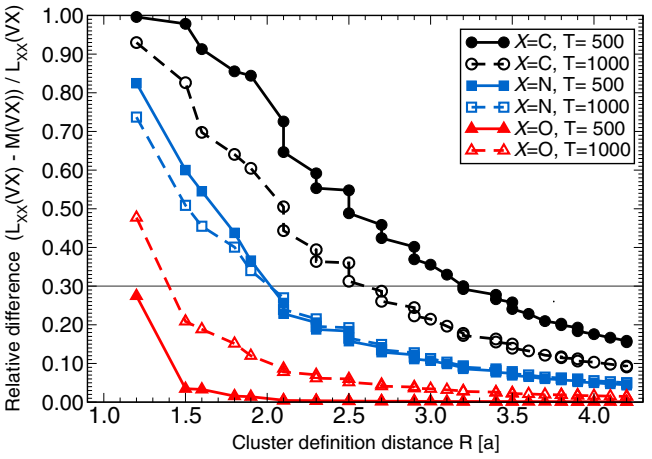

FIG. 2. Relative difference between the pair mobility and the solute diagonal Onsager coefficient for the pair $1 - M(VX)/L_{XX}(VX)$ as a function of the cluster definition distance R, expressed in units of bcc Fe lattice parameter a. Solid lines and filled symbols are for $T = 500$ K; dashed lines and empty symbols are for $T = 1000$ K. The gray line is the threshold under which the mobility is considered a converged quantity. VC pairs are shown in black (circles); VN pairs are shown in blue (squares); and VO pairs are shown in red (triangles).

B. Convergence of the mobility coefficient with respect to cluster size

The VX mobility contribution to the Onsager matrix is computed with the SCMF method, but keeping in the equations only jump frequencies for which X (resp. V) is within some distance R from V (resp. X) both before and after the jump. Obviously, $M(VX)$ depends on the value of R. This distance basically divides all cluster configurations into two categories: V and X form a cluster or V and X are isolated monomers. The whole point of this section is trying to define a meaningful R value. It is observed that as R increases, the mobility of the pair $M(VX)$ converges. This is because as R increases, more and more kinetic trajectories are included in the SCMF calculation, but at some point, the probability of a given trajectory decreases with its length. Then, it should be possible to find an R value such that all kinetic trajectories relevant to the mobility have been included.

For all three solutes, we found $L_{XX}(VX) < L_{VV}(VX)$ over the whole temperature interval. Qualitatively, it means that solute X diffuses slower than V when both form the cluster. As the mobility of the whole cluster requires the motion of each component, it is logical that $M(VX)$ converges towards $L_{XX}(VX)$. Knowing that $L_{XX}(VX)$ converges very fast with R, we take the relative difference between $M(VX)$ and $L_{XX}(VX)$ as an indication of how well the mobility is converged with R. Figure 2 shows this relative difference convergence with respect to R, for each of the three solutes (C in black circles, N in blue squares, and O in red triangles) at

two different temperatures, $T = 500$ K (solid lines with filled symbols) and $T = 1000$ K (dashed lines with open symbols).

Figure 2 shows that convergence of $M(VX)$ is faster for VO pairs than it is for VN pairs, than it is for VC pairs. If we compare first-NN binding energies $E^b(VO) > E^b(VN) > E^b(VC)$, meaning that short kinetic trajectories will have a higher thermodynamic weight for VO pairs than for VC pairs. This is consistent with the observed trend (lower binding implies that long-range kinetic trajectories represent a larger relative contribution). On the other hand, the influence of temperature on the convergence of $M(VX)$ with R is difficult to rationalize qualitatively.

One must be aware that a high R value is not desirable because as R increases, more and more monomer contributions are included in the pair cluster (up to the whole system if R goes to infinity). Thus, the dilute system assumption on which the breakdown of the Onsager matrix relies would not be valid for high R. In this work, we arbitrarily set our convergence criterion to the relative difference between $M(VX)$ and $L_{XX}(VX)$ being less than 30% (gray solid line in Fig. 2), which seems reasonable. In order to have consistent and comparable calculations for each solute, R is chosen from the less converged case: VC pair at $T = 500$ K. In all results below, $R = 3.20a$. Note that the first R value in Fig. 2 is equal to the thermodynamic interaction range ($1.23a$). Thus, a purely thermodynamic definition of cluster radius does not give converged mobility coefficients.

C. Intrinsic flux-coupling ratio for VX pairs

In the previous section, we defined the pair distance R, which relies both on thermodynamic and kinetic properties of the cluster. Using this definition, one can obtain converged kinetic quantities related to the association, mobility, and dissociation of a vacancy-interstitial solute pair cluster. These properties are intrinsic equilibrium properties of the cluster if the system is sufficiently dilute such that all of its internal configurations reach local equilibrium faster than the average time between two association phenomena. There are two flux-coupling ratios in the system under study defined as the off-diagonal coefficient of the Onsager matrix divided by each of the two diagonal coefficients.

It has been shown in Eq. (26) that in the dilute system, all flux-coupling phenomena arise due to the formation of VX pairs. The relative proportions of pairs and monomers will only impact the amplitude of the flux coupling, but not its qualitative nature (positive or negative sign). Because flux coupling is usually studied in out-of-equilibrium conditions (quench, irradiation), it is not possible to estimate the respective concentrations of pairs and monomers in a general way. We thus choose to restrict our discussion to the intrinsic flux-coupling ratio of the VX pair, which will give the sign of the flux coupling. If one knows the respective concentrations of pairs and monomers in a given out-of-equilibrium system, then the data below can be combined with Eq. (26) to compute the magnitude of the flux coupling, and the result is exact in the dilute limit:

$$\frac{L_{\alpha\beta}(VX)}{L_{\beta\beta}(VX)} = \frac{M(VX) + AD_{\alpha\beta}(VX)}{M(VX) + AD_{\beta\beta}(VX)}. \quad (27)$$

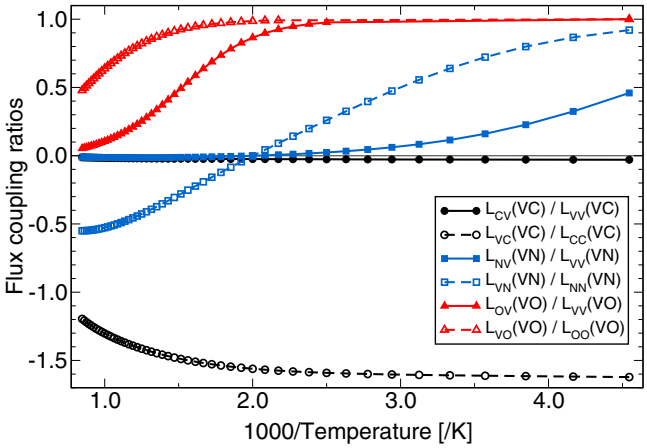

FIG. 3. Flux-coupling ratios related to VX pairs [$L_{XV}(VX)/L_{VV}(VX)$ as solid lines with filled symbols, and $L_{VX}(VX)/L_{XX}(VX)$ as dashed lines with empty symbols] as a function of the inverse temperature. The gray solid line is set at 0 to help distinguish between positive and negative ratios. Colors and symbols relate to the solute: C (black lines with circles), N (blue lines with squares), and O (red lines with triangles).

Figure 3 shows these intrinsic flux-coupling ratios for each of the three VX pairs.

First, it is interesting to note that despite their high binding with V [5], each interstitial solute presents a qualitatively different flux-coupling behavior. Over the whole temperature range, VO pairs (red curves) show a positive flux coupling and both ratios have comparable orders of magnitude. On the contrary, VC pairs (black curves) show a negative flux coupling over the whole temperature range, and both ratios differ by 1 to 2 orders of magnitude. Finally, VN pairs (blue curves) switch from positive flux coupling at low temperature to negative flux coupling at high temperature, with a transition temperature around 550 K. Note that absolute values of $L_{XV}(VX)/L_{VV}(VX)$ are always lower than absolute values of $L_{VX}(VX)/L_{XX}(VX)$. Therefore, we expect the number of vacancies dragged by solute atoms to be larger than the number of solutes dragged by vacancies, for a given driving force. This difference in the behavior of each solute next to a vacancy is attributed to the details of the local energetic landscape around a pair, both because of different binding energies as a function of the vacancy-solute distance [5] and specific saddle-point energies between two configurations [36].

Some deeper, at least qualitative, understanding can be achieved by looking at Eq. (27). The denominator is always positive, so the sign of the flux coupling is governed by the sum $M(VX) + AD_{\alpha\beta}(VX)$. This sum is symmetric with respect to species α and β and this is why both flux-coupling ratios of a given VX pair always have the same sign. The mobility of a cluster being always a positive quantity, only the association/dissociation coefficient can explain a possible negative-flux-coupling behavior. Physically, a cluster associates, and then later on dissociates. The association/dissociation coefficient explains the average relative position of the components of the cluster just before association and just after dissociation, and these two configurations are linked by the way the cluster

moves or, in other words, the way the components of a cluster move altogether.

It is quite simple to visualize this with a substitutional solute vacancy pair on the bcc lattice, in which we assume that the exchange frequency of V with a solute is orders of magnitude lower than the exchange frequency of V with a matrix atom. This way, we can assume that each time V will exchange with the solute, it will then exchange with a matrix atom and separate from the solute. Now, assume that the pair definition distance in this example is the first-NN distance only. V associates with the solutes by jumping to one of its first-NN sites, then V and solute exchange their positions (which is a mobility jump for the pair), and ultimately V migrates away from the solute (dissociation jump). In this system, it is easy to understand that there is a negative flux coupling because solute and vacancy flow in opposite direction, due to the vacancy exchange mechanism, or in other words, the way the vacancy substitutional solute pair diffuses.

Coming back to our interstitial solute vacancy pair, the situation is much more complicated because both of these migrate independently while their migration paths are affected by the complex energetic landscape due to their interactions. Figure 3 tells us about the average result of this correlated motion. There is an interesting trend with first-NN binding energies: high binding energies should result in a high-mobility contribution, which favors positive flux coupling ($M(VX)$ is always positive). Lower binding energies increase the association/dissociation contribution with respect to the mobility contribution, and this can result in negative flux coupling (if $AD_{\alpha\beta}(VX)$ is negative, which is not necessarily the case). Note that the physics of negative flux coupling is purely contained in the association/dissociation contribution: $AD_{\alpha\beta}(VX) = 0$ will always result in positive flux coupling.

D. Effect of second-NN solute jumps around V

In Ref. [36], it is obtained from DFT calculations that interstitial solutes are able to perform second-NN jumps around V, with a low migration barrier. The overall effect on the migration kinetics of a VX pair is hardly predictable. The fast redistribution of X around V randomizes the position of X, which can be thought to erase part of the kinetic correlations, or to have no effect at all on the migration of V.

Figure 4 shows the relative error (difference between calculations that do not take second-NN solute jumps around V into account and calculations that do take them into account) as a function of temperature for three quantities: pair mobility $M(VX)$ (filled triangles) and pair flux-coupling coefficients $L_{XV}(VX)/L_{VV}(VX)$ (solid lines with filled symbols) and $L_{VX}(VX)/L_{XX}(VX)$ (dashed lines with empty symbols). Results are plotted for VC (black curves with circles) and VN (blue curves with squares) pairs because all results for VO pairs are lower than 10^{-3}. Thus, it can be safely concluded that second-NN oxygen jumps around V do not affect the kinetic properties of VO pairs. The gray line is the 30% relative difference threshold used in Fig. 2 as a convergence criterion. The same criterion is used in this discussion.

The results show that second-NN nitrogen jumps around V do not affect much the kinetic properties of VN pairs, at least at temperatures below $T \simeq 1000$ K. For VC pairs, these jumps

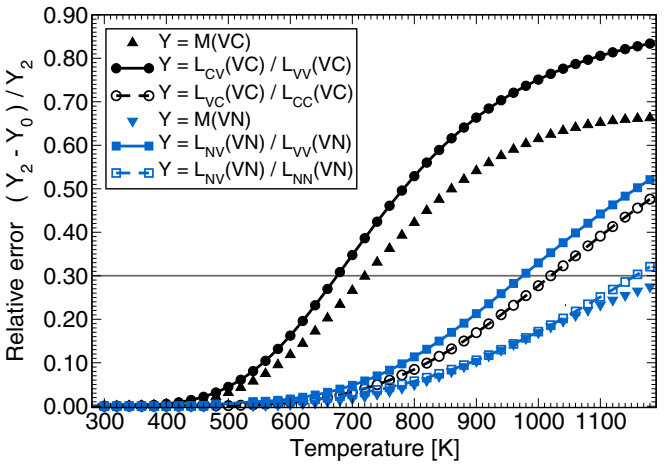

FIG. 4. Temperature variation of the relative error in quantity Y depending on whether second-NN solute jumps around V are included in the calculation (Y_2) or not (Y_0). Quantity Y is either the pair mobility (filled triangles), or a flux-coupling ratio (solid lines with filled symbols and dashed lines with empty symbols, as in Fig. 3). Results are plotted for VC pairs (black lines and circles) and VN pairs (blue lines and squares).

have important effect on the mobility coefficient $M(V\mathrm{C})$ and the flux-coupling coefficient $L_{CV}(V\mathrm{C})/L_{VV}(V\mathrm{C})$, especially at high temperature ($T \geqslant 700$ K). In such conditions, these jumps should be taken into account when computing kinetic properties of VX pairs.

The general conclusion drawn from this plot is that these jumps become more and more important as temperature increases and as the binding energy between V and X decreases (from O to C). The effect of these jumps on the kinetic properties of VX pairs is not spectacular, but it is expected to be much more important for larger cluster, e.g., V_2X, as second-NN solute jumps around vacancies provide low migration energy trajectories that result in an effective displacement of the cluster [36].

IV. DISCUSSION

As a final comment to this paper, we provide a comparison between various models and approximations for the evaluation of cluster kinetic properties. This discussion is illustrated by the example of a VC pair in α-Fe, and five models are being compared with the same set of thermodynamic and kinetic properties, four of which directly stem from previous paragraphs, while the other is a common and convenient approximation found in the literature [4,36,39,50,51]. Note that previous models provide the cluster mobility only, while the SCMF method allows the exact computation of the full Onsager matrix for each cluster. The various kinetic coefficients obtained and discussed below are shown in Fig. 5.

Model I (blue dashed-dotted line) corresponds to the highest barrier approximation [36] which can be summarized this way: Given an energy landscape between two configurations (that may or may not go through multiple stable and/or metastable states), the effective barrier to go between these two configurations is approximated by the energy difference between the most stable state and the most energetic transition

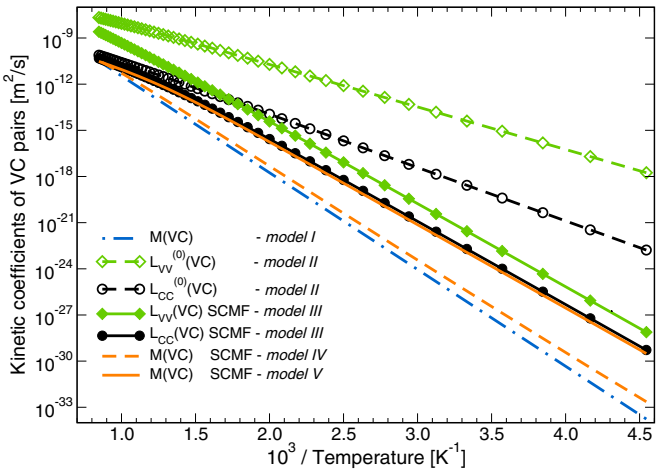

FIG. 5. Various kinetic coefficients as a function of the inverse temperature obtained from different models and approximations (see text for detailed explanation about each model).

state. Model II (green and black dashed lines with empty symbols) are the diagonal VC pair Onsager coefficients in which kinetic correlations were neglected (i.e., all effective interactions ν_σ^{VX} contained in vector $\mathbf{K}$ were set to 0). This model is in fact a thermodynamic average of all possible jump rates for each species. Model III (green and black solid lines with full symbols) uses the same settings as model II, except that this time the effective interactions were given their value as obtained from the SCMF theory [Eq. (19)]. Thus, kinetic correlations up to $3.20a$ range are taken into account, where a is the α-Fe lattice parameter. Kinetic correlations describe the deviation from random diffusion or, in other words, the relative probability of various jump sequences. Comparison between models II and III shows the importance of kinetic correlations, and that a simple thermodynamic average of jump rates predicts kinetic coefficients that are off by several orders of magnitude, especially at low temperature.

Moreover, each species has its own kinetic properties. This is not taken into account in model I, in which only one kinetic coefficient is computed for the pair. To achieve a better understanding of this approximation, it is compared to the mobility contribution of the VC pair, in which the pair distance R has been set equal to the thermodynamic interaction range $1.23a$. The result is labeled model IV (orange dashed line), and it is close to results from the highest barrier approximation (model I): an Arrhenius fit gives a 1.25 eV effective migration energy for model I, and 1.20 eV for model IV. In these two models, the vacancy and the carbon atom are constrained to migrate within distance $R = 1.23a$ from each other. But, we might think that higher-range kinetic trajectories also contribute to the mobility of the pair cluster. Hence, in model V (orange solid line), the pair distance R was increased to $3.20a$, and an Arrhenius fit to this curve gives a lower effective migration energy for the VC pair cluster: 1.08 eV. It is also interesting to note that model V is pretty close to the $L_{CC}(VC)$ coefficient of model III. This is because, as R increases, the mobility contribution converges towards the cluster transport coefficient related to the slowest component, in this case, C. In other words, the slowest species of a cluster limits the overall mobility of the cluster.

V. CONCLUSION

In this paper, we extended the self-consistent mean field calculation of transport coefficients to systems containing multiple migration mechanisms taking place on various sublattices. Then, we proposed a breakdown of the Onsager matrix (valid for dilute systems) into cluster contributions, each of these being itself separated into two contributions: mobility and association/dissociation. The latter contains information about the relative positions of cluster components before association and after dissociation, these two configurations being linked by the atomic details of cluster migration. Analytical expressions for the SCMF equations are provided in the Appendixes. These cluster Onsager matrices are valuable pieces of information that can be used as input for mesoscale simulations.

We applied this formalism to vacancy-interstitial solute pairs (X = C, N, and O) in α-Fe, with DFT based thermodynamic and kinetic parameters from earlier publications. The convergence of the mobility contribution with respect to the cluster definition distance R has been shown, and allows a rigorous definition of this distance relying both on thermodynamics and kinetics. Particularly, these results show that taking R as the thermodynamic interaction range is usually not sufficient to obtain converged kinetic properties.

We investigated cluster flux-coupling ratios, which give the sign of flux couplings in dilute systems. Surprisingly, and despite the fact that each of the three solutes has a highly attractive binding with vacancies, they show different flux-coupling behavior: flux coupling is positive for VO pairs, negative for VC pairs, and positive (negative) for VN pairs below (above) 550 K. These qualitatively different behaviors stem from the specific energetic landscape around VX pairs, and its evolution with respect to the distance between both components. Nevertheless, we found an interesting qualitative trend with first-NN binding energies: high binding energies should result in a high-mobility contribution, which favors positive flux coupling. Lower binding energies increase the association/dissociation contribution with respect to the mobility contribution, and this can result in negative flux coupling. Note that the physics of negative flux coupling is purely contained in the association/dissociation contribution.

For both of these properties (mobility and flux-coupling ratios), we have shown that the effect of the low-activation barrier second-NN jumps of X around V becomes non-negligible for VC pairs (and to a lesser extent VN) at high temperature only ($T \geqslant 700$ K). It does not affect kinetic properties of VO pairs.

Finally, we compared different kinetic approximations for a cluster pair. The common "highest barrier" approximation [4,36,39,50,51] is close to the mobility contribution limited to the thermodynamic interaction range, which is not a converged kinetic quantity as higher-range kinetic trajectories are important in the overall mobility of the cluster. Kinetic correlations reduce cluster transport coefficients by several orders of magnitude compared to a simple thermodynamic average of jump rates. This result alone fully justifies the need for accurate kinetic methods able to compute these kinetic correlation effects in a general and flexible way, for instance, the SCMF.

Despite common geometrical and thermodynamic features, all three solutes show qualitatively different kinetic behaviors in the vicinity of a vacancy. This study demonstrates the general fact that kinetic properties should not be inferred from thermodynamics, as it is sometimes done [52]. The breakdown of the Onsager matrix is a first step towards a comprehensive modeling of cluster properties from the atomic scale [48]. It allows the study of each cluster's kinetic properties independently, and can be combined with other methods able to compute cluster migration paths (e.g., [53]). In future works, we aim at generalizing this method further to clusters containing three components or more.

ACKNOWLEDGMENT

This work was supported by the joint program "CPR ODISSEE" funded by AREVA, CEA, CNRS, EDF, and Mécachrome under Contract No. 070551.

APPENDIX A: ANALYTICAL MATRICES FOR THE COMPUTATION OF VX PAIRS TRANSPORT COEFFICIENTS IN BCC SOLIDS

In this appendix, we provide semianalytical expressions for the calculation of VX cluster transport coefficients on a bcc lattice, as obtained from the SCMF method (Sec. II). Following, we provide expressions for matrices $\mathbf{\Lambda}_0, \mathbf{\Lambda}, \boldsymbol{M}$, and $\boldsymbol{T} = (\boldsymbol{C_1}|\boldsymbol{C_2}) - \mathrm{diag}(\boldsymbol{D})$, where $\mathrm{diag}(\boldsymbol{D})$ is a diagonal matrix whose diagonal elements are the components of vector $\boldsymbol{D}$. From Eqs. (20) and (22), the pair cluster Onsager matrix is

$$\begin{pmatrix} L_{VV}(VX) & L_{VX}(VX) \\ L_{XV}(VX) & L_{XX}(VX) \end{pmatrix} = 2a(\mathbf{\Lambda}_0 + \mathbf{\Lambda} \cdot [(\boldsymbol{C_1}|\boldsymbol{C_2}) - \mathrm{diag}(\boldsymbol{D})]^{-1} \cdot \boldsymbol{M}). \quad \text{(A1)}$$

These matrices are only functions of $W_{ij}^{\alpha} = W_{ji}^{\alpha}$ terms. W_{ij}^{α} denotes the product $\eta_0(\mathbf{n})W(\mathbf{n},\tilde{\mathbf{n}}) = \eta_0(\tilde{\mathbf{n}})W(\tilde{\mathbf{n}},\mathbf{n})$ where α is the jumping species (V or X), V and X are ith NN in configuration $\mathbf{n}$ and jth NN in configuration $\tilde{\mathbf{n}}$. We assumed thermodynamic interactions up to the sixth NN (equivalent distance is $1.23a$), following notations from Refs. [5,36]. Let the distance between V and X at rth-NN position be equal to R, the pair cluster definition distance, set to $R = 2.06a$ in this example. It is a lower value than those used in Sec. III, but it is a compromise between having converged VX mobilities, and not too lengthy expressions so that they can actually be printed. Every configuration in which V and X are kth NN from each other with $6 < k \leqslant r$ is simply denoted as a rth-NN configuration because they all have similar thermodynamic properties (no interaction). Table I explains which jump frequencies should be set to zero in the matrices below to compute a given contribution to the Onsager matrix.

For completeness, Table II gives the Cartesian coordinates of one instance of each effective interaction class, as was obtained from the SCMF calculation. A chemical potential parallel to the [100] direction was used in this calculation, and the numbering of kinetic interaction classes σ is consistent with matrices $\mathbf{\Lambda}$,$(\boldsymbol{C_1}|\boldsymbol{C_2})$, and $\boldsymbol{D}$ below.

Finally, Eqs. (A3)–(A9) are the analytical expressions for the matrices appearing in Eq. (A1), and enable the computation of VX pair cluster transport coefficients:

TABLE I. 17 jump frequencies used in this calculation ($R = 2.06a, 1.23a < r \leqslant R$). For each contribution to the Onsager matrix, "1" indicates that W_{ij}^{α} must be set to its physical value, while "0" indicates that W_{ij}^{α} must be set to zero. The association/dissociation contribution is then obtained as the difference $AD_{\alpha\beta}(VX) = L_{\alpha\beta}(VX) - M(VX)$.

Jump	W_{12}^V	W_{16}^V	W_{12}^X	W_{11}^X	W_{25}^V	W_{2r}^V	W_{25}^X	W_{5r}^V	W_{56}^V
$L_{\alpha\beta}(VX)$	1	1	1	1	1	1	1	1	1
$M(VX)$	1	1	1	1	1	1	1	1	1
Jump	W_{5r}^X	W_{56}^X	W_{6r}^V	W_{6r}^X	W_{rr}^V	$W_{r\infty}^V$	W_{rr}^X	$W_{r\infty}^X$	
$L_{\alpha\beta}(VX)$	1	1	1	1	1	1	1	1	
$M(VX)$	1	1	1	1	1	0	1	0	

$$ {}^t\mathbf{\Lambda} = \begin{pmatrix} W_{12}^V - W_{16}^V & -W_{11}^X \\ 2\,W_{12}^V - 2\,W_{2r}^V & W_{25}^X - W_{12}^X \\ 2\,W_{25}^V - 2\,W_{56}^V & 0 \\ 2\,W_{25}^V - 4\,W_{5r}^V + 2\,W_{56}^V & W_{5r}^X - W_{25}^X \\ 2\,W_{16}^V - 2\,W_{6r}^V & 2\,W_{6r}^X - 2\,W_{56}^X \\ W_{16}^V + 2\,W_{56}^V - 3\,W_{6r}^V & 0 \\ W_{2r}^V - W_{6r}^V & 0 \\ 2\,W_{2r}^V + 2\,W_{6r}^V - 4\,W_{r\infty}^V & 2\,W_{rr}^X - 2\,W_{6r}^X \\ W_{6r}^V - W_{r\infty}^V & 0 \\ 2\,W_{5r}^V - 2\,W_{r\infty}^V & 0 \\ 2\,W_{5r}^V - 2\,W_{r\infty}^V & W_{rr}^X - W_{5r}^X \\ 2\,W_{6r}^V - 2\,W_{rr}^V & W_{r\infty}^X - W_{rr}^X \\ 2\,W_{6r}^V + 2\,W_{rr}^V - 4\,W_{r\infty}^V & 0 \\ 2\,W_{5r}^V - 2\,W_{r\infty}^V & 0 \\ 2\,W_{5r}^V - 2\,W_{r\infty}^V & 0 \\ 2\,W_{5r}^V + 4\,W_{rr}^V - 6\,W_{r\infty}^V & 2\,W_{r\infty}^X - 2\,W_{rr}^X \\ 0 & 0 \\ 2\,W_{6r}^V - 2\,W_{r\infty}^V & 2\,W_{r\infty}^X - 2\,W_{rr}^X \\ W_{6r}^V + 2\,W_{rr}^V - 3\,W_{r\infty}^V & 0 \\ 4\,W_{rr}^V - 4\,W_{r\infty}^V & W_{r\infty}^X - W_{rr}^X \end{pmatrix}, \quad \text{(A2)}$$

TABLE II. Cartesian coordinates of one instance of each kinetic interaction class (in units of $a/2$). The numbering of kinetic interaction classes σ is arbitrary but consistent with matrices $\mathbf{\Lambda}$,$(\boldsymbol{C_1}|\boldsymbol{C_2})$, and $\boldsymbol{D}$ below. A chemical potential gradient parallel to the [100] direction was used in this calculation.

σ	x	y	z	σ	x	y	z	σ	x	y	z	σ	x	y	z
1	1	0	0	6	2	1	1	11	3	1	0	16	3	2	1
2	1	1	0	7	1	2	2	12	2	3	0	17	1	4	0
3	1	2	0	8	2	2	1	13	3	2	0	18	2	3	2
4	2	1	0	9	3	0	0	14	1	3	2	19	3	2	2
5	1	2	1	10	1	3	0	15	2	3	1	20	4	1	0

$$\mathbf{\Lambda}_0(1,1) = 3\left(W_{12}^V + W_{16}^V + 2\,W_{25}^V + W_{2r}^V + 4\,W_{5r}^V + 2\,W_{56}^V + 5\,W_{6r}^V + 12\,W_{rr}^V + 24\,W_{r\infty}^V\right), \tag{A3}$$

$$\mathbf{\Lambda}_0(2,2) = W_{12}^X + W_{11}^X + W_{25}^X + W_{5r}^X + 2\,W_{56}^X + 2\,W_{6r}^X + 9\,W_{rr}^X + 8\,W_{r\infty}^X, \tag{A4}$$

$$\mathbf{\Lambda}_0(1,2) = \mathbf{\Lambda}_0(2,1) = 0, \tag{A5}$$

$$\boldsymbol{M} = \begin{pmatrix} 4\,W_{12}^V - 4\,W_{16}^V & -4\,W_{11}^X \\ 2\,W_{12}^V - 2\,W_{2r}^V & W_{25}^X - W_{12}^X \\ 2\,W_{25}^V - 2\,W_{56}^V & 0 \\ 2\,W_{25}^V - 4\,W_{5r}^V + 2\,W_{56}^V & W_{5r}^X - W_{25}^X \\ W_{16}^V - W_{6r}^V & W_{6r}^X - W_{56}^X \\ W_{16}^V + 2\,W_{56}^V - 3\,W_{6r}^V & 0 \\ W_{2r}^V - W_{6r}^V & 0 \\ W_{2r}^V + W_{6r}^V - 2\,W_{r\infty}^V & W_{rr}^X - W_{6r}^X \\ 4\,W_{6r}^V - 4\,W_{r\infty}^V & 0 \\ 2\,W_{5r}^V - 2\,W_{r\infty}^V & 0 \\ 2\,W_{5r}^V - 2\,W_{r\infty}^V & W_{rr}^X - W_{5r}^X \\ 2\,W_{6r}^V - 2\,W_{rr}^V & W_{r\infty}^X - W_{rr}^X \\ 2\,W_{6r}^V + 2\,W_{rr}^V - 4\,W_{r\infty}^V & 0 \\ W_{5r}^V - W_{r\infty}^V & 0 \\ W_{5r}^V - W_{r\infty}^V & 0 \\ W_{5r}^V + 2\,W_{rr}^V - 3\,W_{r\infty}^V & W_{r\infty}^X - W_{rr}^X \\ 0 & 0 \\ W_{6r}^V - W_{r\infty}^V & W_{r\infty}^X - W_{rr}^X \\ W_{6r}^V + 2\,W_{rr}^V - 3\,W_{r\infty}^V & 0 \\ 4\,W_{rr}^V - 4\,W_{r\infty}^V & W_{r\infty}^X - W_{rr}^X \end{pmatrix}, \tag{A6}$$

$$\boldsymbol{D} = \begin{pmatrix} 4\,W_{12}^V + 4\,W_{16}^V + 4\,W_{12}^X + 4\,W_{11}^X \\ 2\,W_{12}^V + 2\,W_{12}^X + 4\,W_{25}^V + 2\,W_{2r}^V + 2\,W_{25}^X \\ 2\,W_{25}^V + W_{25}^X + 4\,W_{5r}^V + 2\,W_{56}^V + W_{5r}^X + 2\,W_{56}^X \\ 2\,W_{25}^V + W_{25}^X + 4\,W_{5r}^V + 2\,W_{56}^V + W_{5r}^X + 2\,W_{56}^X \\ W_{16}^V + 2\,W_{56}^V + 2\,W_{56}^X + 5\,W_{6r}^V + 2\,W_{6r}^X \\ W_{16}^V + 2\,W_{56}^V + 2\,W_{56}^X + 5\,W_{6r}^V + 2\,W_{6r}^X \\ W_{2r}^V + W_{6r}^V + 2\,W_{6r}^X + 4\,W_{rr}^V + 2\,W_{r\infty}^V + 2\,W_{rr}^X \\ W_{2r}^V + W_{6r}^V + 2\,W_{6r}^X + 4\,W_{rr}^V + 2\,W_{r\infty}^V + 2\,W_{rr}^X \\ 4\,W_{6r}^V + 4\,W_{r\infty}^V + 4\,W_{rr}^X \\ 2\,W_{5r}^V + W_{5r}^X + 4\,W_{rr}^V + 2\,W_{r\infty}^V + 3\,W_{rr}^X \\ 2\,W_{5r}^V + W_{5r}^X + 4\,W_{rr}^V + 2\,W_{r\infty}^V + 3\,W_{rr}^X \\ 2\,W_{6r}^V + 2\,W_{rr}^V + 4\,W_{r\infty}^V + 3\,W_{rr}^X + W_{r\infty}^X \\ 2\,W_{6r}^V + 2\,W_{rr}^V + 4\,W_{r\infty}^V + 3\,W_{rr}^X + W_{r\infty}^X \\ W_{5r}^V + 4\,W_{rr}^V + 3\,W_{r\infty}^V + 3\,W_{rr}^X + W_{r\infty}^X \\ W_{5r}^V + 4\,W_{rr}^V + 3\,W_{r\infty}^V + 3\,W_{rr}^X + W_{r\infty}^X \\ W_{5r}^V + 4\,W_{rr}^V + 3\,W_{r\infty}^V + 3\,W_{rr}^X + W_{r\infty}^X \\ 4\,W_{rr}^V + 4\,W_{r\infty}^V + W_{rr}^X + 3\,W_{r\infty}^X \\ W_{6r}^V + 2\,W_{rr}^V + 5\,W_{r\infty}^V + 2\,W_{rr}^X + 2\,W_{r\infty}^X \\ W_{6r}^V + 2\,W_{rr}^V + 5\,W_{r\infty}^V + 2\,W_{rr}^X + 2\,W_{r\infty}^X \\ 4\,W_{rr}^V + 4\,W_{r\infty}^V + W_{rr}^X + 3\,W_{r\infty}^X \end{pmatrix}, \tag{A7}$$

$$\boldsymbol{C}_1 = \begin{pmatrix}
0 & 4W_{12}^X & 0 & 0 & 0 & 4W_{16}^V & 0 & 0 & 0 & 0 \\
W_{12}^X & 0 & W_{25}^X & 2W_{25}^V + W_{25}^X & 0 & 0 & 0 & 2W_{2r}^V & 0 & 0 \\
0 & W_{25}^X & 0 & 0 & 2W_{56}^X & 2W_{56}^V & 0 & 0 & 0 & W_{5r}^X \\
0 & 2W_{25}^V + W_{25}^X & 0 & 0 & 2W_{56}^V & 2W_{56}^X & 0 & 0 & 0 & 0 \\
0 & 0 & W_{56}^X & W_{56}^V & 0 & 0 & W_{6r}^X & W_{6r}^V + W_{6r}^X & 0 & 0 \\
W_{16}^V & 0 & 2W_{56}^V & 2W_{56}^X & 0 & 0 & W_{6r}^V & 2W_{6r}^X & W_{6r}^V & 0 \\
0 & 0 & 0 & 0 & 2W_{6r}^X & W_{6r}^V & 0 & 0 & 0 & 0 \\
0 & W_{2r}^V & 0 & 0 & W_{6r}^V + W_{6r}^X & W_{6r}^X & 0 & 0 & 0 & W_{rr}^V \\
0 & 0 & 0 & 0 & 0 & 4W_{6r}^V & 0 & 0 & 0 & 0 \\
0 & 0 & W_{5r}^X & 0 & 0 & 0 & 0 & 2W_{rr}^V & 0 & 0 \\
0 & 0 & 0 & 2W_{5r}^V + W_{5r}^X & 0 & 0 & 0 & 2W_{rr}^V & W_{rr}^X & 0 \\
0 & 0 & 0 & 0 & 2W_{6r}^V & 0 & 0 & 0 & 0 & W_{rr}^X \\
0 & 0 & 0 & 0 & 0 & 2W_{6r}^V & 0 & 0 & 0 & 0 \\
0 & 0 & 0 & 0 & 0 & 0 & W_{rr}^X & W_{rr}^V & 0 & 0 \\
0 & 0 & W_{5r}^V & 0 & 0 & 0 & W_{rr}^V & W_{rr}^X & 0 & 0 \\
0 & 0 & 0 & W_{5r}^V & 0 & 0 & 0 & W_{rr}^V + W_{rr}^X & 0 & 0 \\
0 & 0 & 0 & 0 & 0 & 0 & 0 & 0 & 0 & W_{rr}^X \\
0 & 0 & 0 & 0 & W_{6r}^V & 0 & 0 & 0 & 0 & 0 \\
0 & 0 & 0 & 0 & 0 & W_{6r}^V & 0 & 0 & 0 & 0 \\
0 & 0 & 0 & 0 & 0 & 0 & 0 & 0 & 0 & 0
\end{pmatrix}, \tag{A8}$$

$$\boldsymbol{C}_2 = \begin{pmatrix}
0 & 0 & 0 & 0 & 0 & 0 & 0 & 0 & 0 & 0 \\
0 & 0 & 0 & 0 & 0 & 0 & 0 & 0 & 0 & 0 \\
0 & 0 & 0 & 0 & 2W_{5r}^V & 0 & 0 & 0 & 0 & 0 \\
2W_{5r}^V + W_{5r}^X & 0 & 0 & 0 & 0 & 2W_{5r}^V & 0 & 0 & 0 & 0 \\
0 & W_{6r}^V & 0 & 0 & 0 & 0 & 0 & W_{6r}^V & 0 & 0 \\
0 & 0 & 2W_{6r}^V & 0 & 0 & 0 & 0 & 0 & W_{6r}^V & 0 \\
0 & 0 & 0 & 2W_{rr}^X & 2W_{rr}^V & 0 & 0 & 0 & 0 & 0 \\
W_{rr}^V & 0 & 0 & W_{rr}^V & W_{rr}^X & W_{rr}^V + W_{rr}^X & 0 & 0 & 0 & 0 \\
4W_{rr}^X & 0 & 0 & 0 & 0 & 0 & 0 & 0 & 0 & 0 \\
0 & W_{rr}^X & 0 & 0 & 0 & 0 & W_{rr}^X & 0 & 0 & 0 \\
0 & 0 & W_{rr}^X & 0 & 0 & 0 & 0 & 0 & 0 & 2W_{rr}^V + W_{rr}^X \\
0 & 0 & 0 & 0 & 2W_{rr}^X & 2W_{rr}^V & 0 & 0 & 0 & 0 \\
W_{rr}^X & 0 & 0 & 0 & 2W_{rr}^V & 2W_{rr}^X & 0 & 0 & 0 & 0 \\
0 & 0 & 0 & 0 & 0 & 0 & 0 & W_{rr}^V + W_{rr}^X & 0 & 0 \\
0 & W_{rr}^X & W_{rr}^V & 0 & 0 & 0 & W_{rr}^V & W_{rr}^X & W_{rr}^V & 0 \\
0 & W_{rr}^V & W_{rr}^X & 0 & 0 & 0 & 0 & W_{rr}^V & W_{rr}^X & W_{rr}^V \\
0 & 0 & 0 & 0 & 2W_{rr}^V & 0 & 0 & 0 & 0 & 0 \\
0 & 0 & 0 & W_{rr}^V + W_{rr}^X & W_{rr}^X & W_{rr}^V & 0 & 0 & 0 & 0 \\
0 & 0 & 0 & 0 & 2W_{rr}^V & 2W_{rr}^X & 0 & 0 & 0 & 0 \\
2W_{rr}^V + W_{rr}^X & 0 & 0 & 0 & 0 & 2W_{rr}^V & 0 & 0 & 0 & 0
\end{pmatrix}. \tag{A9}$$

APPENDIX B: ANALYTICAL *VX* PAIR MOBILITY COEFFICIENT IN BCC SOLIDS

In bcc solids, the vacancy cannot jump directly from a first-NN position of the interstitial solute to another equivalent position. Thus, the minimal VX solute pair cluster able to migrate must contain first-NN and second-NN VX configurations, which is equivalent to setting the pair cluster definition radius $R = a/\sqrt{2}$, where a is the lattice parameter. In such a

simple model, the mobility of the pair cluster can be expressed analytically with a simple expression of three jump frequencies only (keeping the W_{ij}^{α} notation from previous section, $M(VX)$ is given in $[m^2/s]$):

$$M(VX) = \frac{2\,a^2\left[2\,W_{12}^{V}\left(1+\frac{W_{11}^{X}}{W_{12}^{X}}\right)+6\,W_{11}^{X}+3\,W_{12}^{X}\right]}{4+2\,\frac{W_{11}^{X}+W_{12}^{V}}{W_{12}^{X}}+\frac{W_{12}^{X}+2\,W_{11}^{X}}{W_{12}^{V}}}. \quad \text{(B1)}$$

This expression is provided here as it is easy to use, and it is exact for systems where thermodynamic interactions and kinetic correlations are limited to first NN and second NN. The study of this expression in various limiting cases clearly shows that the slowest species controls the mobility, and that when one species is much faster than the other, the mobility is well approximated by the highest barrier approximation (cf. Sec. IV).

For more realistic systems (i.e., thermodynamic interaction and kinetic interactions beyond second NN), one should turn to the matrices given in the previous appendix.

[1] C. Domain, C. S. Becquart, and J. Foct, Phys. Rev. B **69**, 144112 (2004).
[2] C. J. Först, J. Slycke, K. J. Van Vliet, and S. Yip, Phys. Rev. Lett. **96**, 175501 (2006).
[3] C. C. Fu, E. Meslin, A. Barbu, F. Willaime, and V. Oison, Solid State Phenomena **139**, 157 (2008).
[4] C. L. Fu, M. Krcmar, G. S. Painter, and X.-Q. Chen, Phys. Rev. Lett. **99**, 225502 (2007).
[5] C. Barouh, T. Schuler, C.-C. Fu, and M. Nastar, Phys. Rev. B **90**, 054112 (2014).
[6] T. Schuler, C. Barouh, M. Nastar, and C.-C. Fu, Phys. Rev. Lett. **115**, 015501 (2015).
[7] T. Anthony, Acta Metall. **17**, 603 (1969).
[8] T. R. Anthony, Phys. Rev. B **2**, 264 (1970).
[9] T. R. Anthony, J. Appl. Phys. **41**, 3969 (1970).
[10] T. Anthony, Acta Metall. **18**, 307 (1970).
[11] K. Russell, Prog. Mater. Sci. **28**, 229 (1984).
[12] G. Was, *Fundamentals of Radiation Materials Science* (Springer, Berlin, 2007).
[13] R. Hu, G. D. Smith, and E. A. Marquis, Prog. Nucl. Energy **57**, 14 (2012).
[14] M. Nastar and F. Soisson, Comprehens. Nucl. Mater. **1**, 471 (2012).
[15] A. Barbu and A. Ardell, Scr. Metall. **9**, 1233 (1975).
[16] P. Pareige, B. Radiguet, and A. Barbu, J. Nucl. Mater. **352**, 75 (2006).
[17] T. R. Anthony, *Radiation-Induced Voids in Metals and Alloys*, edited by J. W. Corbett and L. C. Ianiello (US Atomic Energy Commission, Springfield, Varginia, 1972), pp. 630–645 (unpublished).
[18] N. Sakaguchi, M. Endo, S. Watanabe, H. Kinoshita, S. Yamashita, and H. Kokawa, J. Nucl. Mater. **434**, 65 (2013).
[19] L. Messina, Z. Chang, and P. Olsson, Nucl. Instrum. Methods Phys. Res., Sect. B **303**, 28 (2013).
[20] T. Garnier, M. Nastar, P. Bellon, and D. R. Trinkle, Phys. Rev. B **88**, 134201 (2013).
[21] T. Garnier, D. R. Trinkle, M. Nastar, and P. Bellon, Phys. Rev. B **89**, 144202 (2014).
[22] V. Barbe and M. Nastar, Philos. Mag. **86**, 3503 (2006).
[23] V. Barbe and M. Nastar, Phys. Rev. B **76**, 054206 (2007).
[24] V. Barbe and M. Nastar, Philos. Mag. **87**, 1649 (2007).
[25] L. Messina, M. Nastar, and P. Olsson (unpublished).
[26] R. Oriani, Acta Metall. **18**, 147 (1970).
[27] R. McLellan, Acta Metall. **27**, 1655 (1979).
[28] F. D. Fischer, J. Svoboda, and E. Kozeschnik, Modell. Simul. Mater. Sci. Eng. **21**, 025008 (2013).
[29] Y. Wang, D. Connétable, and D. Tanguy, Acta Mater. **103**, 334 (2016).
[30] M. Koiwa, Acta Metall. **22**, 1259 (1974).
[31] L. Mansur, Acta Metall. **29**, 375 (1981).
[32] A. Vehanen, P. Hautojärvi, J. Johansson, J. Yli-Kauppila, and P. Moser, Phys. Rev. B **25**, 762 (1982).
[33] S. Takaki, J. Fuss, H. Kuglers, U. Dedek, and H. Schultz, Radiat. Eff. **79**, 87 (1983).
[34] V. Irmer and M. Feller-Kniepmeier, Philos. Mag. **25**, 1345 (1972).
[35] N. Hashimoto, S. Sakuraya, J. Tanimoto, and S. Ohnuki, J. Nucl. Mater. **445**, 224 (2014).
[36] C. Barouh, T. Schuler, C.-C. Fu, and T. Jourdan, Phys. Rev. B **92**, 104102 (2015).
[37] A. Lidiard, London, Edinburgh, Dublin Philos. Mag. J. Sci. **46**, 1218 (1955).
[38] A. Le Claire, J. Nucl. Mater. **69-70**, 70 (1978).
[39] C.-C. Fu, J. D. Torre, F. Willaime, J.-L. Bocquet, and A. Barbu, Nat. Mater. **4**, 68 (2004).
[40] T. Garnier, V. R. Manga, D. R. Trinkle, M. Nastar, and P. Bellon, Phys. Rev. B **88**, 134108 (2013).
[41] L. Messina, M. Nastar, T. Garnier, C. Domain, and P. Olsson, Phys. Rev. B **90**, 104203 (2014).
[42] V. Barbe and M. Nastar, Philos. Mag. **86**, 1513 (2006).
[43] M. Nastar and V. Barbe, Adv. Eng. Mater. **8**, 1239 (2006).
[44] M. Nastar, V. Y. Dobretsov, and G. Martin, Philos. Mag. A **80**, 155 (2000).
[45] M. Nastar, Philos. Mag. **85**, 3767 (2005).
[46] M. Nastar and V. Barbe, Faraday Discuss. **134**, 331 (2007).
[47] M. Nastar, Phys. Rev. B **90**, 144101 (2014).
[48] T. Schuler, M. Nastar, and T. Jourdan (unpublished).
[49] *Landolt-Börnstein Volume 26: Diffusion in Solid Metals*, edited by H. Mehrer (Springer, Berlin, 1990).
[50] E. Hayward and C.-C. Fu, Phys. Rev. B **87**, 174103 (2013).
[51] P. Liu, W. Xing, X. Cheng, D. Li, Y. Li, and X.-Q. Chen, Phys. Rev. B **90**, 024103 (2014).
[52] J. Svoboda, Y. V. Shan, E. Kozeschnik, and F. D. Fischer, Modell. Simul. Mater. Sci. Eng. **21**, 065012 (2013).
[53] O. A. Restrepo, N. Mousseau, F. El-Mellouhi, O. Bouhali, M. Trochet, and C. S. Becquart, Comput. Mater. Sci. **112**, 96 (2016).